Geophys. J. Int. (2002) **148,** 201–213

Application of regionalized multiplet stripping to retrieval of aspherical structure constraints

R. Widmer-Schnidrig

Cecil H. and Ida M. Green Institute of Geophysics and Planetary Physics, UCSD, La Jolla, CA 92093-0225*, USA*

Accepted 2001 August 17. Received 2001 August 16; in original form 2001 May 4

SUMMARY

A new technique for the analysis of low-frequency seismic recordings is introduced with which constraints on the Earth's large-scale aspherical structure can be obtained. The technique, which we call 'regionalized multiplet stripping', applies multiplet stripping (Gilbert & Dziewonski, *Phil. Trans. R. Soc. Lond., A,* **278,** 187–296, 1975) to sets of seismograms for which sources and receivers share a common great circle. Multiplet stripping applied to such subsets reveals not only the well-known frequency shifts of fundamental modes but also similar frequency shifts for a large number of overtones. Geographical patterns of overtone frequency shifts can subsequently be related to aspherical structure in an identical manner to the fundamental modes. The newly estimated structure coefficients of overtones provide improved depth resolution for the lowest-order aspherical structure. So far we have retrieved degree $s=2$ aspherical structure coefficients for 271 spheroidal overtones with harmonic degree $\ell>10$. In addition, structure coefficients for $s=4$ could be retrieved for a few well-excited low-n branches. For the fundamental modes, we find very good agreement with single-record peak frequency analyses. Predictions from recent 3-D mantle models generally agree well with our new structure coefficients.

Key words: free oscillations, mantle structure, spheroidal overtones.

1 INTRODUCTION

The methods used to analyse low-frequency seismic data in a normal-mode framework are of interest because they hold the promise of directly constraining lateral variations in density independent of variations in compressional and shear wave velocities. Since the buoyancy force experienced by density anomalies drives mantle convection, images of the density variations are the crucial link between seismology and geodynamics, and are essential for understanding the style of mantle convection. The methods used to analyse normal-mode spectra fall into two groups. The first group is concerned with the analysis of isolated modes with low harmonic degree ℓ. For these modes the effect of aspherical structure can be fully specified with a small set of so-called structure coefficients and these coefficients can be estimated non-linearly from the observed spectra. The most widely used technique is iterative spectral fitting which, when applied to large data sets, has allowed reliable estimation of structure coefficients up to spherical harmonic degree $s=4$ (Ritzwoller *et al.* 1986, 1988; Giardini *et al.* 1987, 1988; Widmer *et al.* 1992; He & Tromp 1996; Resovsky & Ritzwoller 1998). Higher-order structure coefficients have also been estimated in several of these papers, though the values of the different groups do not agree well.

A new and promising technique estimates the structure coefficients linearly using an autoregressive technique to first estimate the splitting matrix (Masters *et al.* 1999).

Among the modes suitable for these two methods are the anomalously split modes which sample the inner core. Many low-ℓ mantle modes have also been analysed successfully, but the overall number of modes analysed remains small ($\sim$90).

For fundamental modes with high harmonic degree ($\ell>10$), aspherical structure no longer leads to observable splitting of the spectrum. The $2\ell+1$ singlets that make up the multiplet are too numerous and the broadening caused by attenuation leads to too much overlap. What is seen instead in the spectra is an apparent shift of the peak frequency away from the degenerate frequency. The asymptotic theory for modes with short wavelength (high ℓ) in smooth structures developed by Jordan (1978) predicts this behaviour and relates the shift to the average structure underlying the great circle connecting source and receiver. In essence, the high- (low-) frequency singlets interfere constructively on a great circle with faster (slower) than average properties, while destructive interference cancels the signals from the low- (high-) frequency singlets.

* Now at: Black Forest Observatory, Heubach 206, D-77709 Wolfach, Germany. E-mail: widmer@geophys.uni-stuttgart.de

Observations of peak frequency shifts of fundamental spheroidal modes are readily made from spectra of single recordings since fundamental modes contribute the largest signal. This technique was pioneered by Masters *et al.* (1982). However, application to overtones is only feasible for a very limited number of modes that fall half way between two fundamental modes (e.g. ${}_2S_{10}$ and ${}_2S_{12}$). This leads to the situation where the only normal modes contributing to aspherical structure inversions are either low-ℓ overtones or high-ℓ fundamental modes (e.g. Romanowicz & Roult 1986; Smith & Masters 1989).

In this paper, we present a new technique that allows extraction of the peak shifting pattern of high-ℓ overtones. Since the asymptotic theory of Jordan (1978) applies equally to fundamental modes and overtones, the interpretation of the overtone peak shifts is straightforward.

Long-period seismic data can also be interpreted in a surface wave context. To estimate surface wave dispersion the individual branches must first be isolated. This separation can be accomplished on a regional scale in the frequency–wavenumber domain by the use of a network of sensors (e.g. Nolet 1975; Cara 1979). On a global scale, however, overtones were initially only incorporated in full waveform inversions (e.g. Woodhouse & Dziewonski 1984, 1986). Waveform inversions use all signals in the (ω, ℓ) plane. However, since fundamental modes and overtones are modelled simultaneously in the time domain, and the former are typically much more excited than the latter, one expects that only the structures sampled by the fundamental modes will be well resolved. The highly non-linear relation between structure perturbations and seismic waveforms further complicates any inference.

Inversions are greatly facilitated if the different overtone branches can be isolated and their dispersion measured individually. Early approaches were based on variable filtering (Cara 1973) and were applied successfully to isolate the fundamental mode branch (e.g. Roult *et al.* 1990). Stutzmann & Montagner (1993, 1994) proposed a technique to extract path-averaged dispersion of overtone branches. However, their technique makes rather restrictive assumptions regarding the data and thus is only applicable to a small number of paths. Recently, van Heijst and Woodhouse (1997) have introduced a mode-branch stripping method that lends itself to applications to large data sets and that can be fully automated (van Heijst and Woodhouse 1999). However, the frequency band over which this method can separate the branches rapidly narrows with increasing overtone number. For the first overtone, the band is approximately 4–20 mHz, for the second overtone, 6–25 mHz, for the third overtone, 12–25 mHz and for the fourth, 20–25 mHz. While this method can lead to a significant improvement in both lateral and depth resolution in the upper mantle and transition zone, the modes situated in a large fraction of the (ω, ℓ) plane that sample the lower mantle and outer core cannot be analysed or used to constrain the mantle structure. Fig. 1 summarizes the location of the signals in the (ω, ℓ) plane that can be analysed with the various normal-mode methods. Regionalized multiplet stripping, as we shall demonstrate, can retrieve the signature of aspherical structure from many of the remaining modes in the (ω, ℓ) plane below 10 mHz.

2 REGIONALIZED MULTIPLET STRIPPING

Ideally, multiplet stripping gives an unbiased estimate of the multiplet degenerate frequency. An essential prerequisite is that the seismograms used sample the Earth evenly. If our goal is to estimate the degenerate frequency of the multiplet, this prerequisite is the source of major concern regarding bias.

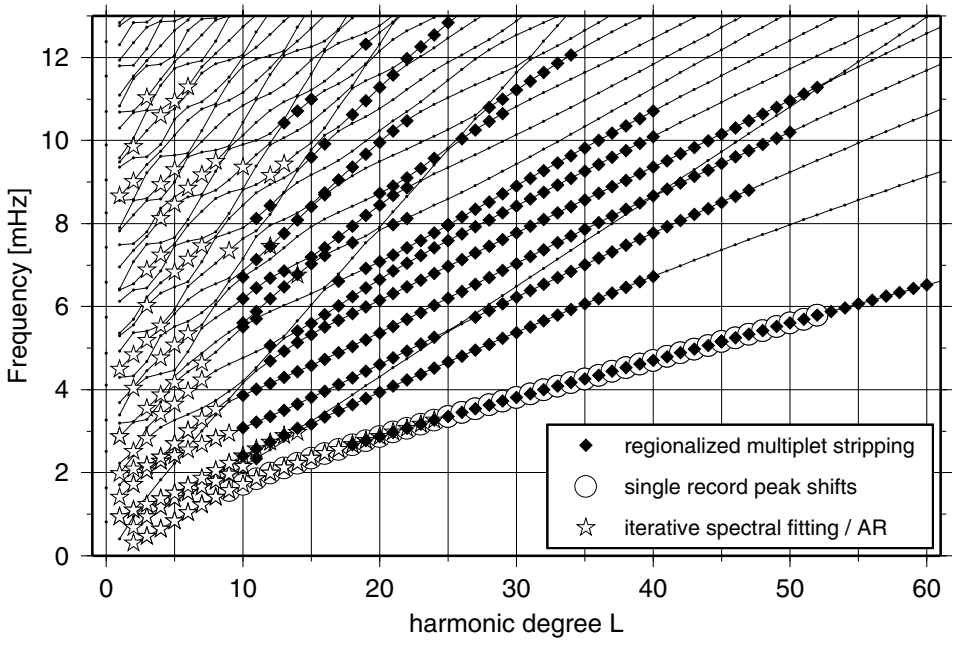

Figure 1. Dispersion diagram for spheroidal modes and model PREM. The modes that can be analysed with either iterative spectral fitting or the autoregressive (AR) technique are towards the low-ℓ side. Peak shift measurements from single records are only feasible for fundamental modes. Regionalized multiplet stripping works for most high-ℓ overtones, except of course the Stoneley and inner core Stoneley modes.

Since for the large majority of modes multiplet stripping is the only technique that can be used to estimate their degenerate frequency, such a bias may remain undetected and lead to biased models of the spherically averaged Earth.

In the course of establishing a new degenerate frequency data set, we were led to try multiplet stripping on subsets of records for which sources and receivers share a common great circle. From the asymptotic analysis by Jordan (1978) we know that multiplets with high harmonic degree ℓ (short wavelength) are predominantly sensitive to the structure underlying the great circle connecting source and receiver. Thus we expect that multiplet stripping of high-ℓ modes applied to records that share a common great circle will yield a frequency estimate that is representative of the structure along the great circle. Given this link between the average structure underneath a great circle and the observed frequency shift, it is straightforward to devise a procedure that accounts for the effect of heterogeneous mantle structure explicitly and yields an unbiased degenerate frequency: we can step through all possible great circle orientations and apply multiplet stripping to the set of records that most closely samples this great circle. The frequencies obtained from all the strips can then be corrected for a geographical pattern and an unbiased mean obtained. As a byproduct of this strategy to obtain unbiased degenerate frequency estimates we also obtain a map of peak frequency shifts that we can interpret in terms of aspherical structure much like fundamental mode peak frequency measurements.

3 OUTLINE OF THEORY

3.1 Multiplet stripping

Multiplet stripping (Gilbert & Dziewonski 1975) linearly estimates multiplet resonance functions from a set of observed spectra. On a spherically symmetric, non-rotating Earth, the observed spectrum of ground acceleration at the jth station $u_j(\omega)$ is a weighted sum of multiplet resonance functions $c_k(\omega)$,

$$u_j(\omega) = A_{jk} c_k(\omega) \,. \tag{1}$$

Given an earth model [in our case PREM (Dziewonski & Anderson 1981)] the multiplet excitation A_{jk} for a particular earthquake–receiver pair can be computed. An important aspect of this calculation is that only the value of the eigenfunction of the mode at the source and receiver are needed. The eigenfrequency, however, does not enter A. For any spherically symmetric earth model, mode eigenfunctions factor into model-dependent radial eigenfunctions and a spherical harmonic function describing angular variations. While computation of the radial eigenfunction still requires an earth model, we find that if the radial eigenfunctions are grossly wrong the multiplet strips are degraded in quality but still informative. The best example are modes near Stoneley mode branch-crossings above 10 mHz, which are incorrectly predicted by current models. PREM predicts ${}_5S_{54}$ to be a Stoneley mode yet multiplet stripping is able to retrieve a clear resonance function, indicating that ${}_5S_{54}$ is actually an upper mantle mode. This illustrates how insensitive multiplet stripping is with regard to errors in the radial eigenfunctions. The only *a priori* information needed are the source and receiver coordinates together with the source mechanism.

Multiplet stripping consists of solving eq. (1) for the resonance functions $c_k(\omega)$:

$$\hat{c}_k(\omega) = A^{-1}_{kj} u_j(\omega) \,. \tag{2}$$

The estimated resonance functions $\hat{c}_k(\omega)$ are termed *multiplet strips*. $\mathbf{A}^{-1}$ denotes the generalized inverse of $\mathbf{A}$, which we compute using singular-value decomposition for multiple right-hand sides (Golub & Reinsch 1971). We apply multiplet stripping to narrow frequency bands containing no more than five adjacent fundamental spheroidal modes. Over such $\sim$0.5 mHz wide bands, the source mechanism and hence $\mathbf{A}$ can be considered to be independent of frequency. This leads to an efficient numerical algorithm, since we need to decompose $\mathbf{A}$ only once. The multiplet index k runs over all multiplets in the chosen frequency band and we typically include both spheroidal and toroidal modes. In the numerical implementation, the spectra $u(\omega)$ are obtained by fast Fourier transformation of the discretely sampled seismograms. This makes the left-hand side of eq. (1) a matrix with the row index running over the frequencies of our target interval. Since multiplet excitations are always real, the matrix $\mathbf{A}$ is also real, while both the spectra $u(\omega)$ and the strips $\hat{c}(\omega)$ are complex.

We choose identical time windows for all records and a record length of $1 \times Q$ cycles of the target mode, where Q is the quality factor of the mode as predicted by PREM. Since we are not interested in high-Q overtones we always start the time window on the event time and do not make use of the Earth as an attenuation filter.

In a subsequent step, we estimate the peak frequency from the complex strip $\hat{c}_k(\omega)$ by fitting the spectrum of a decaying cosinusoid with unknown frequency, attenuation, initial amplitude and phase (Masters & Gilbert 1983). Since the spectra that make up the left-hand side of eq. (1) are Hanning tapered for reduction of spectral leakage, we also incorporate an identical taper into the model resonance function. From the signal-to-noise ratio in the strips, the error in the frequency estimate can be computed (Dahlen 1982).

A further concern with the implementation of multiplet stripping is that the records come from different instruments that have not only differing gains but that also distort the signal differently. Rather than deconvolving the data using the instrument transfer function (an inherently unstable operation), we have selected the instrument/recording unit with the narrowest frequency response contained in our data set and bandpass-filtered all records to that response. Since all modern sensors/recording units have a broad-band frequency response, this bandpass-filter operation can be accomplished with a very short convolution filter. In this way we are guaranteed to perform only numerically stable operations.

Since the different earthquakes in our database vary by a factor of 300 in seismic moment ($0.1 \leq M_0 \leq 30 \times 10^{20}$ Nm), the matrix $\mathbf{A}$ is completely dominated by the rows from the largest events. This effectively downgrades our geographical coverage. As a countermeasure we choose to normalize all spectra by their rms amplitude. In this way, we downweight spectra with high signal-to-noise ratio from large events but gain improved coverage. Since many of the large events have complex and poorly known source mechanisms, this weighting also reduces the influence of these events.

After this balancing of the rows, the matrix $\mathbf{A}$ may still be ill-conditioned. This occurs if a mode is included where the

eigenfunction is vanishingly small throughout the upper mantle and crust. Such modes cannot be excited by earthquakes and thus the corresponding column in **A** is very small. By constructing the generalized inverse of **A** from its singular-value decomposition, one can find a stable inverse by judiciously rejecting singular values. Since this procedure is not easily automated we have chosen a different strategy to deal with excessively small columns and simply eliminate the problematic modes from our mode catalogue all together. We have eliminated the Stoneley modes of the core–mantle boundary and the inner core boundary as well as modes confined to the inner core. The former two can be readily identified based on their group velocity and the latter group has a quality factor close to the average Q_μ value of PREM in the inner core (~ 85).

A further concern with multiplet stripping is leakage from unmodelled modes immediately adjacent to the chosen frequency band. Such tails of flanks from nearby modes can be particularly large for fundamental modes and can lead to biased frequency estimates. To avoid this problem we have performed separate multiplet stripping experiments for each mode with the chosen frequency window centred on the target mode. In this way we avoid having to estimate the frequency of a spectral peak near the edges of our target frequency band where leakage effects can be severe.

3.2 Interpretation of frequency shifts

As introduced above, regionalized multiplet stripping applies multiplet stripping to sets of seismograms that share a common great circle. Here we address how such measurements can be interpreted. Let the frequency shift $\delta\bar{\omega}$ on the great circle with pole at (Θ, Φ) be

$$\delta\hat{\omega}_k(\Theta, \Phi) = \omega_k(\Theta, \Phi) - \bar{\omega}_k\,,$$

where ω_k is the peak frequency estimated from the regionalized strips and $\bar{\omega}_k$ is the mean frequency of the multiplet. This frequency shift can, to zeroth order, be interpreted as a great circle average of the splitting function of the kth multiplet (Jordan 1978).

The splitting function $f(\theta, \phi)$ summarizes the aspherical structure sensed by one multiplet,

$$f(\theta, \phi) = \sum_{\substack{s=0\\ \text{even}}}^{2\ell} \sum_{t=-s}^{s} c_s^t\, Y_s^t(\theta, \phi)\,, \tag{4}$$

where the c_s^t in this expansion are the structure coefficients (defined in eq. 11 below) of the multiplet ${}_nS_\ell$. The splitting function has frequency as units and its value at a particular location (θ_0, ϕ_0) can be interpreted as the degenerate frequency perturbation that the multiplet would experience if the spherically averaged Earth structure were identical to the structure located underneath (θ_0, ϕ_0).

The great circle average of the splitting function is

$$\delta\hat{\omega}(\Theta, \Phi) = \frac{1}{2\pi} \oint_{\Theta,\Phi} d\Delta \sum_{\substack{s=0\\ \text{even}}}^{2\ell} \sum_{t=-s}^{s} c_s^t\, Y_s^t(\theta, \phi)\,, \tag{5}$$

where $\oint$ denotes integration around the great circle with a pole at (Θ, Φ). Integration of eq. (5) can be carried out analytically (Backus 1964) and with P_s denoting the Legendre polynomial of the order of s we obtain

$$\delta\hat{\omega}(\Theta, \Phi) = \sum_{\substack{s=0\\ \text{even}}}^{2\ell} \sum_{t=-s}^{s} P_s(0) c_s^t\, Y_s^t(\Theta, \Phi)\,. \tag{6}$$

Eq. (6) states that the great circle average of a spherical harmonic function $Y_s^t(\theta, \phi)$ is its value at the location of the pole (Θ, Φ) multiplied by $P_s(0)$. The Legendre polynomial $P_s(0)$ vanishes at the origin for odd values of s which has the well-known consequence that the spectra of isolated multiplets are insensitive to aspherical structure of odd harmonic degree. For increasing harmonic degree $s = 0, 2, 4, 6, \ldots$ the magnitude of $P_s(0)$ decreases and is $1, -1/2, 3/8, -5/16, \ldots$. This decrease in $P_s(0)$ effectively means that the shorter the wavelength of the structure, the smaller its signature in the peak frequency shifts. In other words, a map of peak-frequency shifts is a low-pass filtered version of the splitting function.

We parametrize Earth structure as a superposition of a spherically symmetric reference model M_0 and a small volumetric perturbation δm,

$$M_\oplus(r, \theta, \phi) = M_0(r) + \delta m(r, \theta, \phi)\,. \tag{7}$$

The perturbation can be expanded in spherical harmonics

$$\delta m(r, \theta, \phi) = \sum_{s=0}^{S_{\max}} \sum_{t=-s}^{s} \delta m_s^t(r)\, Y_s^t(\theta, \phi) \tag{8}$$

and if we restrict heterogeneous perturbations to be isotropic we obtain for the elements of the model vector

$$\delta m_s^t(r) = [\delta\mu_s^t(r), \delta\kappa_s^t(r), \delta\rho_s^t(r)]^{\mathrm{T}}\,. \tag{9}$$

Apart from volumetric perturbations, the first-order discontinuities can also be deformed. The height of the nth perturbed interface above the unperturbed discontinuity can be described with an expansion of the form

$$h_n(\theta, \phi) = \sum_{s=0}^{S_{\max}} \sum_{t=-s}^{s} h_{ns}^t(r)\, Y_s^t(\theta, \phi)\,. \tag{10}$$

Having a mathematical description for heterogeneous Earth structure, we proceed and ask how such structure affects normal-mode spectra. Woodhouse & Dahlen (1978) show that to first order the structure coefficients c_s^t of the kth multiplet are linearly related to heterogeneous volumetric structure as well as interface topography through

$${}_kc_s^t = \int_0^a {}_k\mathbf{M}_s(r)^{\mathrm{T}} \cdot \delta m_s^t(r) r^2\, dr - \sum_{n=1}^{N} {}_kB_{ns} \cdot h_{ns}^t \cdot r_n^2\,, \tag{11}$$

where ${}_k\mathbf{M}_s$ denotes the sensitivity kernels. These kernels depend on the parameters of the unperturbed model, the eigenfunction of the mode and the harmonic degree s of the structure but are independent on the azimuthal order.

$${}_k\mathbf{M}_s(r) = [{}_kM_s(r), {}_kK_s(r), {}_kR_s(r)]^{\mathrm{T}}\,. \tag{12}$$

The second term in eq. (11) is the contribution of boundary topography where the index n labels the first-order discontinuities.

Eqs (6) and (11) can be combined to yield an explicit relation between the expansion coefficients of heterogeneous structure $[\delta\mathbf{m}_s^t(r), h_s^t]$, on the one hand, and the observed great circle

averages, $\delta\hat{\omega}_k(\Theta, \Phi)$, on the other hand:

$$\delta\hat{\omega}_k(\Theta, \Phi) = \sum_{s,t} P_s(0)\, Y_s^t(\Theta, \Phi) \times \left[\int_0^a \mathbf{M}_s(r)^{\mathrm{T}} \delta\mathbf{m}_s^t(r) r^2\, dr - \sum_n {}_k B_{ns} h_{ns}^t r_n^2 \right]. \quad (13)$$

Aspherical structure can now be estimated in two ways. In either case, we start by binning our records for all possible great circle pole locations, moving the centre of the bin in regular intervals over the surface of the Earth. With a bin radius of 20° (and allowing for some overlap of the bins) we obtain 92 bins for which we can carry out separate multiplet stripping experiments for each mode. For the bins that contain enough records to make eq. (1) overdetermined, we solve eq. (1) and interactively estimate the peak frequency of the target multiplet from the strips. At this point the two methods diverge: in the first method, we use the ≤ 92 peak frequency estimates from a target multiplet and employ eq. (6) to estimate the structure coefficients for that mode (see Section 5). Subsequently, the structure coefficients from all multiplets can be used in eq. (11) to estimate the radial distribution of aspherical structure. Note that structure of degree s and order t depends only on the structure coefficients of the same degree and order. This leads to separate linear inverse problems for each (s, t)-pair.

The second method is based on eq. (13) and estimates aspherical structure directly from the original peak frequency estimates. This involves solving one large linear system of equations. The number of data, N, equals the number of peak frequency measurements. The number of unknowns, M, is the product of the number of layers in the model, the number of parameters (e.g. rigidity, bulk modulus and density) and the number of structure coefficients. The advantage of this approach is that one arrives at a model with laterally variable resolution that reflects the data coverage in Fig. 2.

4 THE DATA SET

Our data set consists of 12 000 recordings of the IRIS, GEOSCOPE, MEDNET and GEOFON networks and includes only events from 1991 to 1998. While the station distribution has become more uniform over the last few years, the stations with high-quality, low-frequency recordings are still primarily continental sites. Therefore, we had to discard many recordings from smaller events and stations on oceanic islands. Together with the uneven distribution of earthquake sources we obtain a data set which necessarily samples the Earth very unevenly. The density of the poles of all great circles for the 12 000 seismograms in our edited database is shown in Fig. 2.

We have performed a number of controls with our seismic data to ensure internal consistency. The traces were inspected visually and defects flagged. This includes elimination of large aftershocks, instrument calibration signals and noise bursts owing to environmental influences on sensors. The next step involves low-pass filtering and decimating the data to a sampling interval of 20 s followed by removal of the tidal signal. Detiding is performed by fitting harmonics with the frequencies of the major tidal constituents to the time series. This leaves us with the data in a form suitable for multiplet stripping. Since we make use of both amplitude and phase information contained in the earthquake signals, we need to verify that we have a good model of both the earthquake source and the instrument response. We do this by comparing our records with synthetic seismograms computed for a 1-D reference earth model. Any serious problems with the source mechanism, the instrument response (i.e. reversed polarities), the timing of the records or the station coordinates will lead to a poor fit and can be caught in this way. Typical variance reductions for our 1-D synthetic seismograms vary between 65 and 90 per cent, which translate to very good fits in the time domain. We verify the good fit of data and synthetic traces by visual inspection.

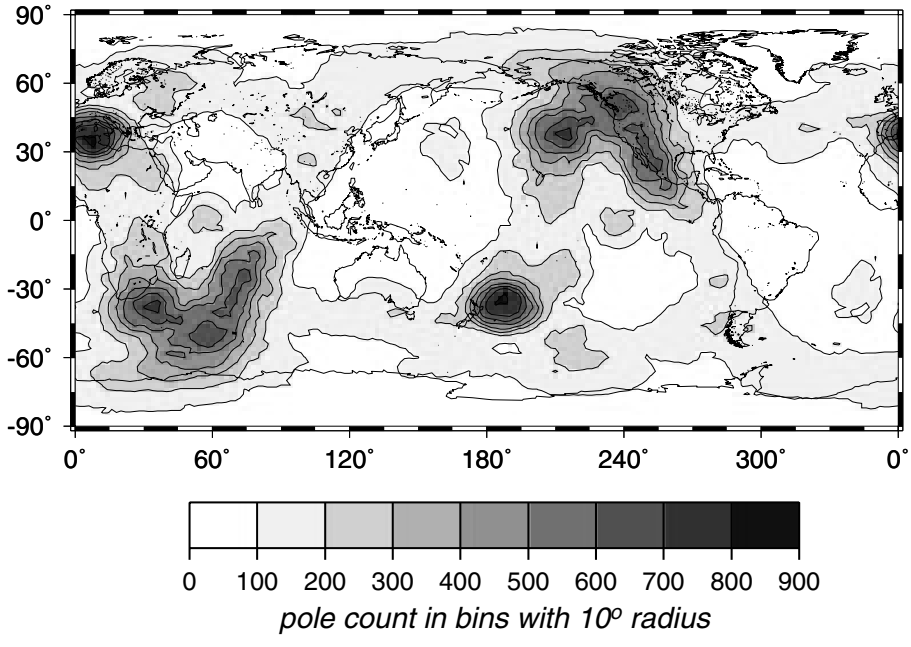

Figure 2. Great circle pole density for the 12 000 records in the data set used for this study. The records are from 144 events between 1991 and 1998. The values displayed are the pole counts in circular caps with 10° radius.

5 ESTIMATING STRUCTURE COEFFICIENTS FROM PEAK FREQUENCY MEASUREMENTS

To estimate structure coefficients as an intermediate step on the way to structural models is advantageous since it enables us to inspect along-branch consistency. Structure coefficients are expected to vary smoothly along a branch since the eigenfunctions differ only slightly between adjacent modes and thus sample similar structures. Thus along-branch consistency provides a powerful quality check. In addition, the use of structure coefficients greatly simplifies the inversion for heterogeneous structure. Eq. (6) provides the link between our peak frequency measurements and the structure coefficients. On the left-hand side of eq. (6) we have the spherical harmonic expansion of a function with coefficients $P_s(0)c_s^t$. Since the peak frequency measurements are associated with an error, we only fit them to within some prescribed tolerance (Parker 1989). A sensible choice to select among the family of models that achieve this misfit is to select the smoothest model $g(\theta, \phi)$. We define R as the roughness of a function on the unit sphere:

$$R = \int\int \left[\nabla_1^2 g(\theta, \phi)\right]^2 d\Omega \tag{14}$$

where ∇_1^2 denotes the surface Laplacian operator. The smoothest model can then be identified as that for which R is minimal.

An alternative approach to estimating structure coefficients uses spherical harmonic splines (Parker 1989). These splines are the smoothest function under the measure eq. (14) that connects a set of points on a sphere. Since the splitting function of an isolated multiplet is an even function, we use even spherical harmonic splines (G. Masters, private communication, 1999). For data points with associated errors we can find a smooth function that fits the data to within a prescribed tolerance. The advantage is that the interpolating function exhibits no extrema in areas where no data are present. Each spherical harmonic spline has a representation in terms of an infinite sum of regular spherical harmonic functions and, in our procedure of estimating structure coefficients of a particular degree and order, we simply take the corresponding expansion coefficients of our spline function. We obtain an expansion for the peak frequency shifts as a function of the pole location,

$$\delta\hat{\omega}(\Theta, \Phi) = \sum_{\substack{s=0 \\ \text{even}}}^{\infty} \sum_{t=-s}^{s} \omega_s^t Y_s^t(\Theta, \Phi)\,. \tag{15}$$

Comparing eqs (6) and (15), we see that all we need to do to obtain the structure coefficients c_s^t is to divide the expansion coefficients of the peak frequency shifts ω_s^t by $P_s(0)$. Structure coefficients estimated is this way still contain the signal from the Earth's hydrostatic ellipticity. Since ellipticity of figure constitutes an axisymmetric degree $s=2$ structure, it only enters the structure coefficient c_2^0. The correction we have applied is (Dahlen & Tromp 1998, eq. 16.221)

$$c_2^0(\text{ellip}) = 4\sqrt{\frac{4\pi}{5}}\, a\omega_0 \left(1 - \frac{3}{4\ell(\ell+1)}\right), \tag{16}$$

where a denotes the ellipticity parameter of Dahlen & Sailor (1979).

In order to propagate the errors in the peak frequency measurements to the structure coefficients we have used a bootstrapping technique (Efron & Tibshirani 1986). In a first step we perturb each peak frequency estimate ($f_i \pm \sigma_i$) by a random amount drawn from a normal distribution of zero mean and variance σ_i^2. In a second step we exactly fit a spherical harmonic spline function to these perturbed frequency shifts and retain the spherical harmonic expansion coefficients of this spline function (eq. 15). Repeating these two steps 100 times, we obtain 100 estimates for each structure coefficients. The bootstrap estimate of the structure coefficients and their errors are then given by the mean and standard deviations of the 100 estimates.

From the c_0^0 coefficients we obtain an estimate of the multiplet degenerate frequency in which bias owing to uneven sampling of aspherical structure is greatly reduced. This provides a valuable check on degenerate frequency estimates obtained with regular multiplet stripping.

5.1 Bias due to cap averaging

Ideally, all records included in a regionalized stripping experiment sample the same great circle. Given the uneven distribution of sources and receivers, on the one hand, and given the large number of records needed to strip for weakly excited overtones, on the other hand, we are forced to perform some binning of our records. By binning records where the great circle pole falls within a circular cap of a given radius, we effectively increase the data coverage at the price of some loss in resolution. In addition, the retrieved structure coefficients are expected to be biased low. This bias has been estimated in Fig. 3 where we have plotted the spherical harmonic expansion coefficients for a circular cap of variable cap radius. Binning the data is equivalent to convolving the splitting function with the spherical cap of constant amplitude. For our preferred cap size of 20° radius we expect degree $s=2$ structure coefficients to be biased low by 10 per cent and degree $s=4$ coefficients to be biased low by 30 per cent. Since the distribution of great circle poles within each spherical cap is not even, the actual bias may differ somewhat. The bottom line is that a 10 per cent bias is well within our error bars for the degree $s=2$ structure coefficients (see below).

6 RESULTS

Application of regionalized multiplet stripping to our data set of 12 000 records is successful for a large number of modes. We start with the fundamental mode branch since we have independent structure coefficient estimates for these modes from single-record peak frequency measurements (e.g. Masters *et al.* 1982; Romanowicz & Roult 1986; Smith & Masters 1989) and from surface wave analyses (e.g. Wong 1989; Montagner & Tanimoto 1990; Trampert & Woodhouse 1995; Laske & Masters 1996; Ekström *et al.* 1997).

In Fig. 4 the raw strips are shown for the fundamental spheroidal mode ${}_0S_{45}$ with a frequency of 5.15 mHz. All strips are normalized to a unit maximum amplitude. Multiplet stripping failed to extract a clean resonance function for two cap locations only. For this mode, multiplet stripping seems to fail once the number of records in a bin falls below $\sim$100. Considering that the mean (median) number of records per bin is 530 (430) one could reduce the cap radius in an attempt to resolve shorter-wavelength structure.

As an example of a mantle overtone, we show the strips for the mode ${}_7S_{25}$ with a frequency of 7.96 mHz (Fig. 5). This

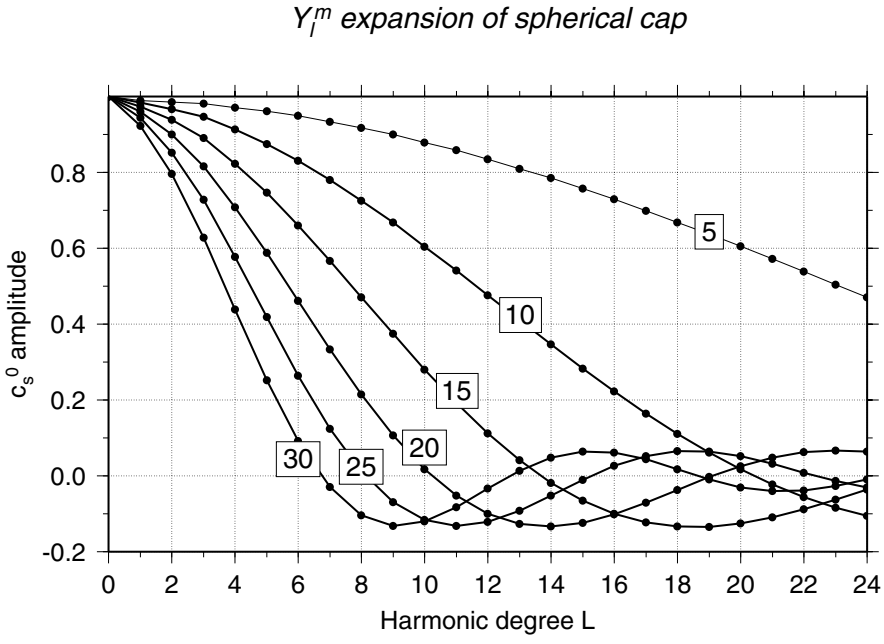

Figure 3. Estimation of bias in structure coefficient estimates owing to binning of data. Shown are the spherical harmonic expansion coefficients of a spherical cap with unit amplitude and variable radius. The cap is centred on the North pole so that only spherical harmonics with azimuthal order $t=0$ contribute. The spherical harmonics are normalized such that a δ-function has equal amplitude at all degrees. The different curves are labelled with the cap radius in degrees. For a cap radius of 20° we expect our estimate of the degree $s=2$ structure coefficients to be biased low by 10 per cent and for $s=4$ by 30 per cent.

mode is sensitive to structure throughout the entire mantle. For this mode, multiplet stripping failed to extract a clean resonance function for ~25 per cent of the bins. We attribute this failure to a lack of signal, since it mostly occurs in bins with few records. The variation in the peak location is clearly visible. Bins for which eq. (1) is not overdetermined (i.e. the number of modes in the frequency band is larger than the number of seismograms in the bin) have been discarded from this plot. This was the case for seven bins. Around ~450 records seem to be required in a bin before ${}_7S_{25}$ can be isolated from neighbouring modes. Increasing the bin radius may produce more robust degree $s=2$ structure coefficients. The mean (median) number of records per bin for this mode are 633 (533).

From the strips with sufficiently high signal-to-noise ratio (shown in Figs 4 and 5) we have estimated the peak frequency for each bin. The signature of large-scale mantle structure in such measurements is best seen when plotting the peak frequency shifts at the location of the corresponding great circle pole. Figs 6 and 7 show the resulting maps for ${}_0S_{45}$ and ${}_7S_{25}$. A coherent large-scale pattern is evident. This is also true for ${}_7S_{25}$ where rather large holes in the data coverage are present. Where such holes exist we discard structure coefficients for $s=4$ or greater.

From the interactively assigned noise level in each strip, a formal error, σ, in the peak frequency can be computed (Dahlen 1982). The lower map in Fig. 6 is a 'signal' map. The symbol sizes are proportional to f/σ where $f\pm\sigma$ is the peak frequency and its assigned error in a particular bin. Comparison with Fig. 2 shows that the two are correlated. We note, however, that the most densely populated bins off New Zealand do not produce the strips with the highest signal-to-noise ratio. We speculate that the complex structures around the pacific rim, which are sampled by this group of great circles, leads to complications in the spectra. In fact, we often see hints of split multiplet strips for this great circle. When estimating peak frequencies from such complicated spectra, the model of a single decaying cosinusoid is often inadequate. This leads to a large unmodelled residue that raises the estimate of the noise level and hence the error of the peak frequency estimate.

Our procedure, exemplified with the above two modes, has been applied to all multiplets below 13 mHz and structure coefficients estimated. Modes with harmonic degree $\ell<10$ have been excluded, as they certainly do not satisfy the asymptotic criteria $s\ll\ell$. Restricting ourselves to modes with $\ell\geq10$ we have practically removed all modes with any sensitivity to inner core structure. This is desirable as we need not worry about anomalously split modes for which multiplet stripping is known to yield biased frequency estimates. The results for degree $s=2$ and the branches $n=0$, 5 and 7 are summarized in Figs 8–10. For $s=4$ the structure coefficients for the second pseudo-branch are shown in Fig. 11. Also shown with the estimated structure coefficients are the predictions of model SCB10L18 (G. Masters, private communication, 1999). Model SCB10L18 is a mantle model derived from the travel times of long-period body waves, surface wave dispersion and normal-mode structure coefficients. The effect of the Earth's hydrostatic ellipticity has been subtracted from the observed c_2^0 structure coefficients using eq. (16) whereas the contribution of the crust has been computed based on the model CRUST5.1 (Mooney *et al.* 1998) and is added to the predictions of model SCB10L18. Note, however, that none of the structure coefficients obtained in the current study entered the construction of SCB10L18. The good agreement is encouraging as we can expect the new constraints to be consistent with previous observations and also because we can expect the degenerate frequencies to be largely free of bias from uneven sampling of aspherical structure.

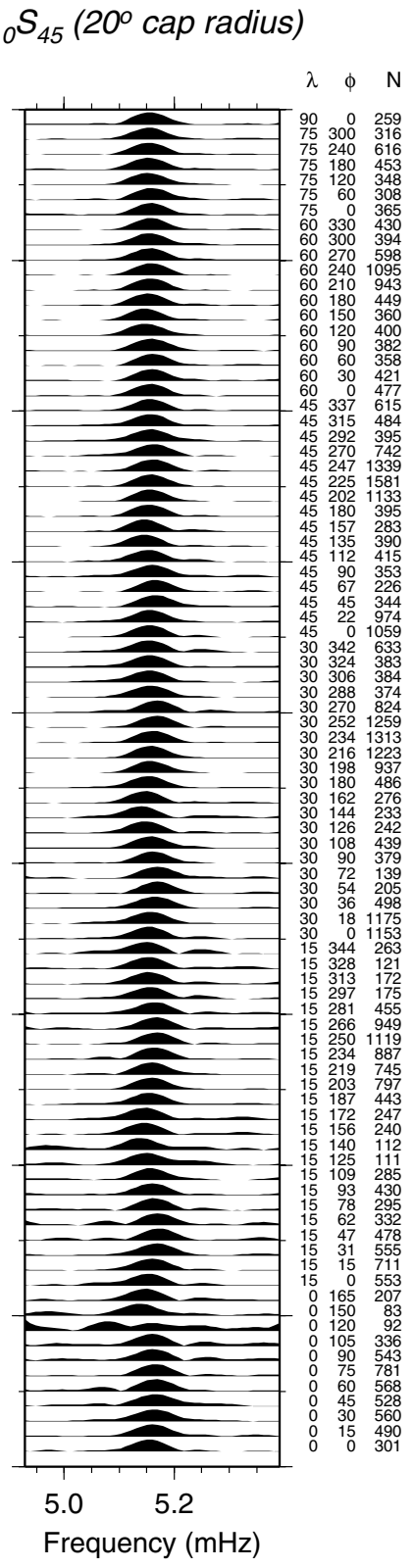

Figure 4. Regionalized multiplet strips for mode $_0S_{45}$. The latitude λ and longitude ϕ of the cap position are given to the right of each strip. The third column gives the number of records N that are included in the strip of a particular bin. This frequency band contains 36 spheroidal and 17 toroidal modes. The figure shows how multiplet stripping is capable of isolating a target mode and conveys the signal level in the strips from which the peak frequency measurements are made. See text for details.

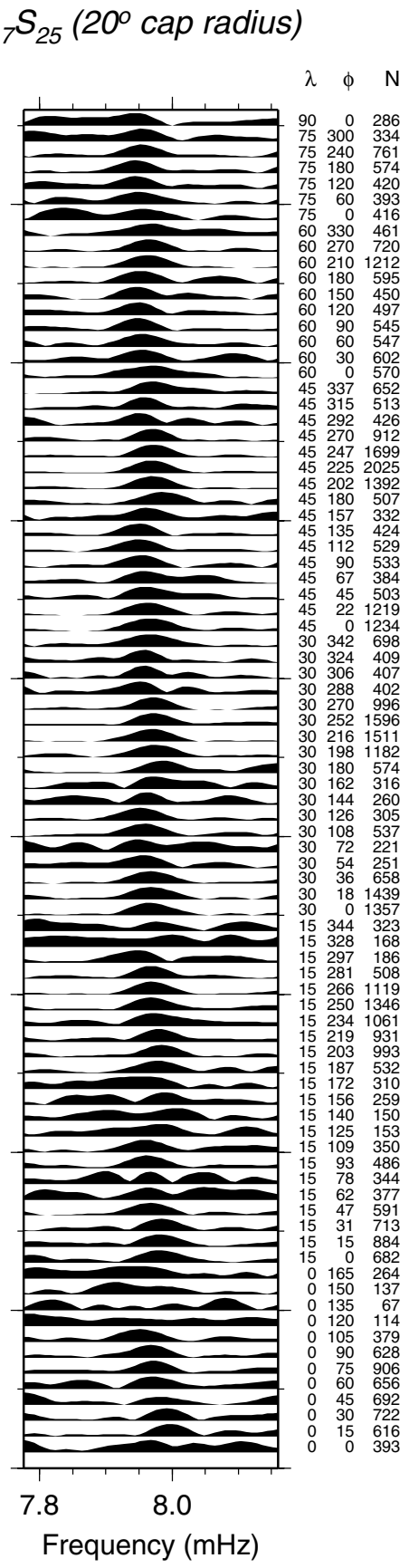

Figure 5. Strips for mode $_7S_{25}$ obtained from regionalized multiplet stripping. The frequency band used for the strips contains 43 spheroidal and 23 toroidal modes. See Fig. 4 for details.

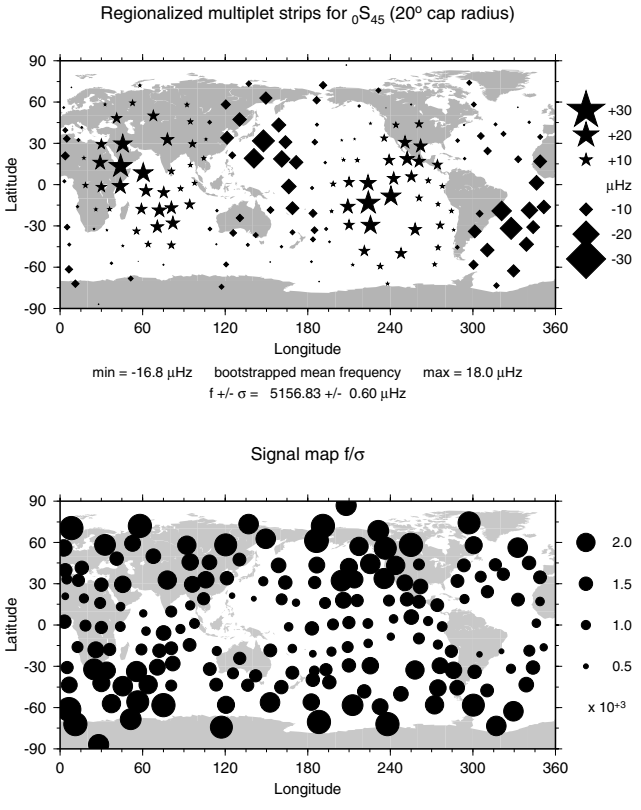

Figure 6. Peak frequency shifts obtained from regionalized multiplet stripping for mode $_0S_{45}$ (upper panel). The individual peak frequency measurements were made from the strips shown in Fig. 4. The symbols are plotted at the mean pole locations of all records that fall into a particular bin. Stars and diamonds indicate positive and negative frequency shifts, respectively. Frequency shifts are proportional to symbol size and the extremal values are given below the figure. The inverse of the errors of the estimated peak frequency shifts is shown in the lower map. A weak correlation with Fig. 2 can be seen.

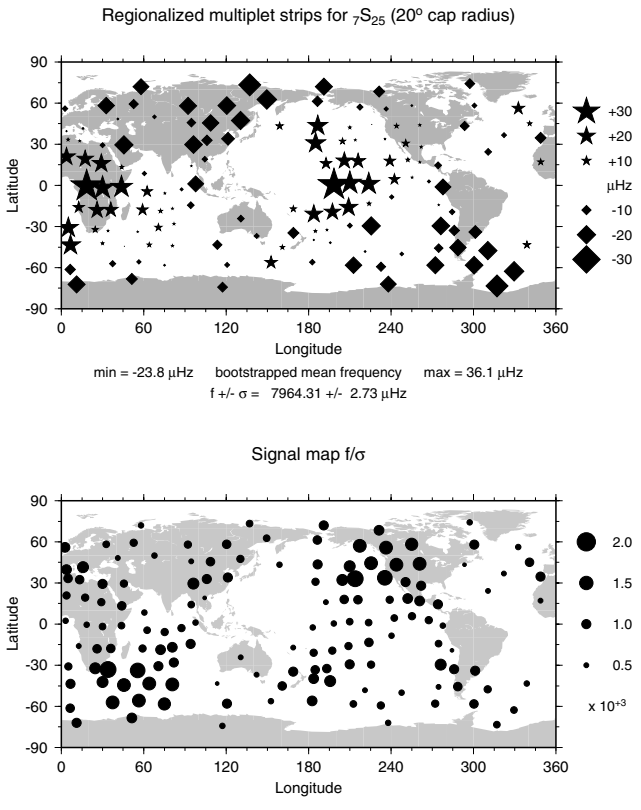

Figure 7. Peak frequency shifts for mode $_7S_{25}$ obtained from regionalized multiplet stripping (upper panel). The individual peak frequency measurements are made from the strips shown in Fig. 5. A large-scale pattern in the frequency shifts is apparent despite some large gaps in the data. Because of these gaps, we do not believe that degree $s=4$ structure can be reliably estimated. The lower panel shows again a 'signal map'. We note, that the strips with the highest signal-to-noise ratio do not coincide with the best sampled great circle where the pole is NE of New Zealand (see Fig. 2). This great circle passes through northern Chile and follows the north Pacific rim all the way to Sumatra. Thus half of this great circle follows convergent plate boundaries. In the strips belonging to this great circle we often find large residues, which we attribute to the complex structures sampled by waves sampling this great circle. The criterion for the validity of our asymptotic theory ($s \ll \ell$) is probably violated on this great circle.

Comparing Figs 8–11, the necessarily smooth trends of the branches appear with very different degrees of clarity. For the fundamental modes the trends of the branches are unambiguous—a result of the fact that this branch is generally very well excited and that the sensed upper mantle structure is relatively large in amplitude. At the other extreme is the $_7S_\ell$ branch for $s=2$ (Fig. 10). This branch is on average only feebly excited and it is predominantly sensitive to the comparably homogeneous lower mantle. Hence the scatter along the branch is relatively large and its deviation from zero hardly significant.

In Table 2 the degenerate frequencies are given. While these values can be expected to be largely free from bias owing to uneven sampling they may still contain bias from coupling to nearby multiplets. However, since the frequency separation to neighbouring modes (and thus the coupling strength) is different for every multiplet along a branch, we expect that multiplet–multiplet coupling does not lead to systematic bias for entire branches.

6.1 Toroidal modes

Since about half the records in our data set come from horizontal component seismograms we have also tried regionalized multiplet stripping on toroidal modes. However, we find that the procedure was only successful for the fundamental mode branch, $_0T_\ell$. For toroidal overtones the global coverage is too uneven. This is no surprise since very often vertical component seismograms from island stations are of rather high quality, while horizontal components are extremely noisy and must be discarded. We still included the horizontal component seismograms in the regionalized multiplet stripping experiments (left-hand side of eq. 1) since they also help to separate spheroidal overtone branches with different polarization of the surface particle motion. To avoid bias from the unmodelled signal on the horizontal components, we also always include the toroidal modes on the right-hand side of eq. (1).

7 APPRAISAL OF THE STRUCTURE COEFFICIENTS

Table 1 gives the amount of signal (initial variance) and the misfit of model SCB10L18. Let us introduce the new index i that uniquely identifies a quadruplet of indices (n, ℓ, s, t) such that $c_i \pm \sigma_i$ denotes the structure coefficients c_s^t and its standard

Table 1. Fit of model SCB10L18 to observed c_2^l structure coefficients. g_i and g_f are defined in eqs (17) and (18), respectively. N gives the total number of coefficients for a branch. Since degree $s=2$ structure comprises five structure coefficients for every multiplet, the number of multiplets in a branch is $N_{\text{modes}}=N/5$.

Branch	g_i	g_f	N
0	6.91	4.38	195
1	2.26	1.46	100
2	2.07	1.50	110
3	3.15	1.84	65
4	2.09	1.74	105
5	2.36	1.98	150
6	2.07	1.60	110
7	2.24	1.76	85
8	1.73	1.61	45
9	2.71	2.06	50
10	2.54	2.11	50
11	1.76	1.37	30
12	3.27	2.48	35
13	3.82	2.88	10
14	2.18	1.94	5
all	3.57	2.43	1145

error of the multiplet ${}_nS_\ell$. Also let $\tilde{c}_i$ denote the matching structure coefficient predicted for model SCB10L18. We now introduce g_i as a measure of the amount of signal available initially,

$$g_{\text{i}} = \sqrt{\frac{1}{N}\sum_{i=1}^{N}\left(\frac{c_i}{\sigma_i}\right)^2}. \tag{17}$$

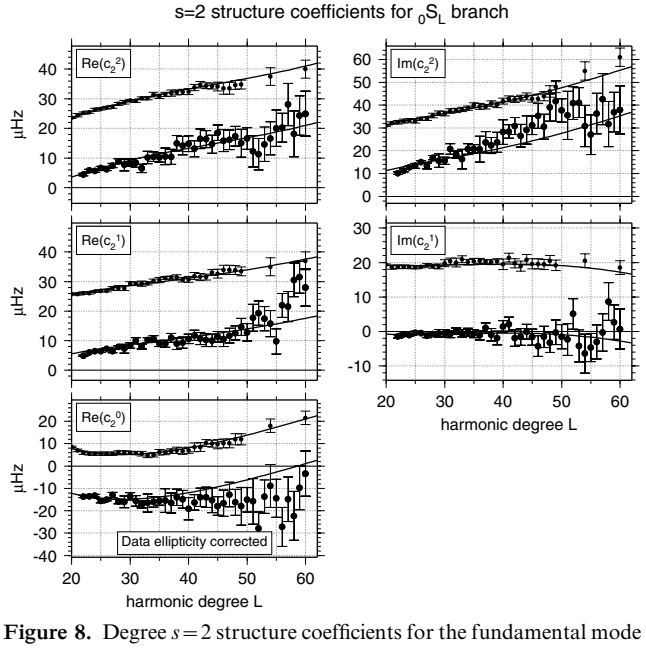

Figure 8. Degree $s=2$ structure coefficients for the fundamental mode branch ${}_0S_\ell$. The lower set of observations in each frame are the results from regionalized multiplet stripping. The upper data set is from single-record peak frequency analyses (Smith & Masters 1989) and is offset by $+20$ μHz. Superimposed on both data sets are the predicted values for model SCB10L18 (G. Masters, personal communications, 1999). See text for details.

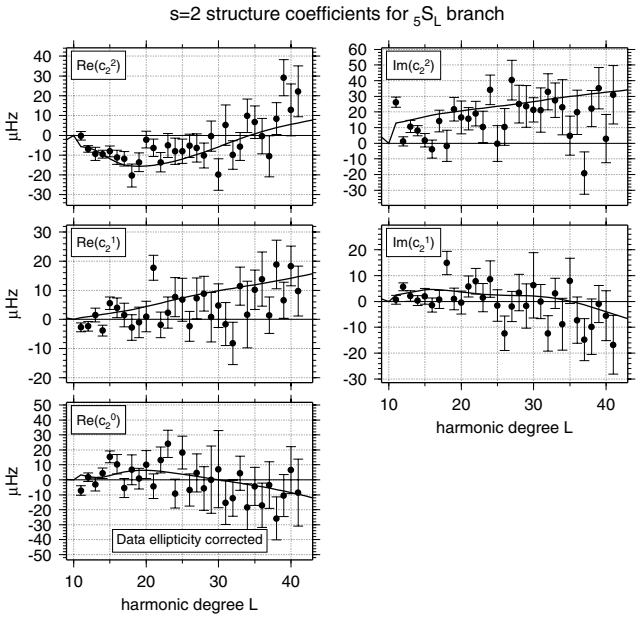

Figure 9. Same as in Fig. 8 but for the ${}_5S_\ell$ branch. Model SCB10L18 seems to predict this branch very well.

Our corresponding measure of the final misfit of model SCB10L18 is g_f.

$$g_{\text{f}} = \sqrt{\frac{1}{N}\sum_{i=1}^{N}\left(\frac{c_i-\tilde{c}_i}{\sigma_i}\right)^2}. \tag{18}$$

A concise way to quantify the amount of added information contained in the newly estimated structure coefficients is to perform *ranking* and *winnowing* of the data (Gilbert 1971) and to compare the number of significant Earth data (sEd) with relative errors less than a given threshold. For a compilation of recently published structure coefficients of 75 mantle-sensitive

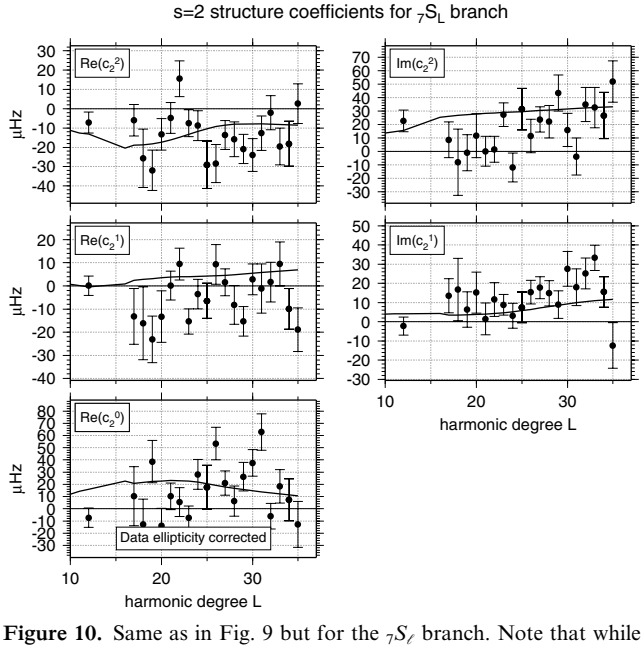

Figure 10. Same as in Fig. 9 but for the ${}_7S_\ell$ branch. Note that while the coefficients exhibit considerable scatter they are not inconsistent.

Table 2. Estimated multiplet degenerate frequencies in μHz.

Mode	f	σ	Mode	f	σ
${}_0S_{18}$	2673.52	0.14	${}_0S_{19}$	2775.76	0.20
${}_0S_{20}$	2875.52	0.21	${}_0S_{21}$	2975.95	0.05
${}_0S_{22}$	3074.19	0.06	${}_0S_{23}$	3170.42	0.16
${}_0S_{24}$	3265.20	0.19	${}_0S_{25}$	3359.23	0.23
${}_0S_{26}$	3451.29	0.23	${}_0S_{27}$	3543.16	0.29
${}_0S_{28}$	3633.65	0.19	${}_0S_{29}$	3724.37	0.56
${}_0S_{30}$	3815.18	0.25	${}_0S_{31}$	3905.11	0.22
${}_0S_{32}$	3994.53	0.68	${}_0S_{33}$	4082.22	0.36
${}_0S_{34}$	4171.84	0.32	${}_0S_{35}$	4261.15	0.32
${}_0S_{36}$	4350.37	0.30	${}_0S_{37}$	4439.59	0.42
${}_0S_{38}$	4528.63	0.44	${}_0S_{39}$	4617.91	0.50
${}_0S_{40}$	4706.96	0.48	${}_0S_{41}$	4797.12	0.51
${}_0S_{42}$	4886.43	0.52	${}_0S_{43}$	4976.59	0.56
${}_0S_{44}$	5064.98	0.65	${}_0S_{45}$	5156.83	0.60
${}_0S_{46}$	5246.89	0.61	${}_0S_{47}$	5335.74	0.75
${}_0S_{48}$	5427.73	0.81	${}_0S_{49}$	5517.36	0.73
${}_0S_{50}$	5607.66	0.78	${}_0S_{51}$	5699.22	1.24
${}_0S_{52}$	5788.65	1.06	${}_0S_{53}$	5881.16	1.13
${}_0S_{54}$	5972.47	1.20	${}_0S_{55}$	6064.50	1.36
${}_0S_{56}$	6156.39	1.01	${}_0S_{57}$	6247.17	1.05
${}_0S_{58}$	6339.33	1.43	${}_0S_{59}$	6434.61	1.69
${}_0S_{60}$	6526.92	1.33	${}_1S_{11}$	2346.17	0.19
${}_1S_{15}$	3172.89	1.18	${}_1S_{16}$	3340.84	1.02
${}_1S_{17}$	3493.39	0.84	${}_1S_{18}$	3643.75	0.61
${}_1S_{19}$	3792.23	0.91	${}_1S_{20}$	3939.97	0.76
${}_1S_{21}$	4085.64	0.61	${}_1S_{22}$	4231.47	0.80
${}_1S_{23}$	4376.25	1.16	${}_1S_{24}$	4521.03	1.16
${}_1S_{25}$	4662.65	1.10	${}_1S_{26}$	4809.11	1.38
${}_1S_{27}$	4952.77	1.59	${}_1S_{28}$	5088.65	1.56
${}_1S_{29}$	5233.02	1.53	${}_1S_{30}$	5373.06	1.78
${}_1S_{31}$	5513.54	2.08	${}_1S_{32}$	5652.36	2.33
${}_1S_{33}$	5788.81	2.06	${}_1S_{34}$	5929.20	2.90
${}_1S_{35}$	6061.83	2.37	${}_1S_{36}$	6192.96	3.00
${}_1S_{37}$	6331.98	3.30	${}_1S_{38}$	6465.34	2.65
${}_1S_{39}$	6594.33	3.40	${}_1S_{40}$	6728.29	3.85
${}_2S_{10}$	2403.95	0.37	${}_2S_{11}$	2572.04	0.25
${}_2S_{12}$	2737.21	0.82	${}_2S_{13}$	2896.99	0.55
${}_2S_{14}$	3065.81	0.85	${}_2S_{27}$	5746.13	0.85
${}_2S_{28}$	5903.81	1.10	${}_2S_{29}$	6068.14	1.28
${}_2S_{30}$	6228.56	1.17	${}_2S_{31}$	6385.16	1.13
${}_2S_{32}$	6541.09	1.49	${}_2S_{33}$	6697.19	1.34
${}_2S_{34}$	6852.39	1.44	${}_2S_{35}$	7011.91	2.31
${}_2S_{36}$	7164.41	2.45	${}_2S_{37}$	7318.55	2.07
${}_2S_{38}$	7473.00	1.81	${}_2S_{39}$	7623.39	2.66
${}_2S_{40}$	7774.94	2.50	${}_2S_{41}$	7921.24	3.89
${}_2S_{42}$	8072.22	4.79	${}_2S_{43}$	8219.54	4.06
${}_2S_{44}$	8360.54	4.24	${}_2S_{45}$	8508.96	4.44
${}_2S_{46}$	8656.20	4.83	${}_2S_{47}$	8807.27	5.10
${}_3S_{10}$	3082.12	0.41	${}_3S_{11}$	3219.52	0.53
${}_3S_{12}$	3361.36	0.41	${}_3S_{13}$	3507.55	0.55
${}_3S_{14}$	3656.20	0.53	${}_3S_{15}$	3810.98	0.59
${}_3S_{16}$	3966.85	0.65	${}_3S_{17}$	4124.01	0.60
${}_3S_{18}$	4283.80	0.67	${}_3S_{19}$	4446.13	0.67
${}_3S_{20}$	4608.98	0.88	${}_3S_{21}$	4771.58	0.75
${}_3S_{22}$	4932.87	0.85	${}_3S_{23}$	5098.42	0.76
${}_3S_{24}$	5262.94	0.81	${}_3S_{41}$	8823.12	2.57
${}_3S_{42}$	8976.89	2.41	${}_3S_{43}$	9138.26	2.30
${}_3S_{44}$	9290.13	2.43	${}_3S_{45}$	9441.41	2.94
${}_3S_{46}$	9603.01	2.74	${}_3S_{47}$	9750.64	2.46
${}_3S_{48}$	9908.12	3.87	${}_3S_{49}$	10 052.90	3.48
${}_3S_{50}$	10 206.65	3.49	${}_4S_{10}$	3864.07	0.63
${}_4S_{11}$	4007.03	0.71	${}_4S_{12}$	4153.64	0.71
${}_4S_{13}$	4292.05	1.04	${}_4S_{14}$	4435.30	0.81
${}_4S_{15}$	4585.08	1.08	${}_4S_{16}$	4729.85	1.04

Table 2. (*Continued.*)

Mode	f	σ	Mode	f	σ
${}_4S_{17}$	4885.32	1.14	${}_4S_{18}$	5043.66	1.05
${}_4S_{19}$	5200.63	1.53	${}_4S_{20}$	5362.19	1.26
${}_4S_{21}$	5526.07	1.29	${}_4S_{22}$	5695.97	1.38
${}_4S_{23}$	5861.48	1.34	${}_4S_{24}$	6028.67	1.49
${}_4S_{25}$	6197.23	1.58	${}_4S_{26}$	6365.49	1.24
${}_4S_{27}$	6535.54	1.73	${}_4S_{28}$	6702.65	1.86
${}_4S_{29}$	6872.95	1.30	${}_4S_{30}$	7038.11	1.30
${}_4S_{31}$	7204.41	2.12	${}_4S_{32}$	7369.39	1.58
${}_4S_{33}$	7536.51	1.87	${}_4S_{34}$	7700.08	1.83
${}_4S_{35}$	7859.58	1.78	${}_4S_{36}$	8019.95	1.48
${}_4S_{37}$	8184.38	1.48	${}_4S_{38}$	8342.15	2.15
${}_4S_{39}$	8499.51	2.34	${}_4S_{40}$	8663.48	2.81
${}_5S_{12}$	4696.82	0.48	${}_5S_{13}$	4925.46	1.02
${}_5S_{14}$	5136.40	0.77	${}_5S_{15}$	5327.26	1.12
${}_5S_{16}$	5505.95	1.09	${}_5S_{17}$	5669.85	1.28
${}_5S_{18}$	5829.20	1.96	${}_5S_{19}$	5988.49	2.17
${}_5S_{20}$	6152.22	1.88	${}_5S_{21}$	6310.38	2.18
${}_5S_{22}$	6473.56	1.85	${}_5S_{23}$	6635.43	1.79
${}_5S_{24}$	6800.78	2.32	${}_5S_{25}$	6965.94	1.92
${}_5S_{26}$	7132.66	1.79	${}_5S_{27}$	7291.93	2.22
${}_5S_{28}$	7455.36	2.08	${}_5S_{29}$	7616.88	2.41
${}_5S_{30}$	7778.52	2.60	${}_5S_{31}$	7941.78	2.35
${}_5S_{32}$	8099.06	2.06	${}_5S_{33}$	8253.59	2.54
${}_5S_{34}$	8407.77	3.84	${}_5S_{35}$	8570.59	2.82
${}_5S_{36}$	8726.95	3.44	${}_5S_{37}$	8884.50	2.89
${}_5S_{38}$	9043.70	3.10	${}_5S_{39}$	9200.63	3.12
${}_5S_{40}$	9360.49	3.77	${}_5S_{41}$	9511.31	3.40
${}_5S_{42}$	9679.32	3.10	${}_5S_{43}$	9835.77	4.64
${}_5S_{44}$	9989.46	3.55	${}_5S_{45}$	10 151.42	2.94
${}_5S_{46}$	10 307.00	3.31	${}_5S_{47}$	10 476.61	3.61
${}_5S_{48}$	10 638.30	3.84	${}_5S_{49}$	10 796.93	3.45
${}_5S_{50}$	10 962.40	3.25	${}_5S_{51}$	11 115.99	3.32
${}_5S_{52}$	11 282.07	2.65	${}_6S_{14}$	5413.08	1.29
${}_6S_{15}$	5600.20	1.20	${}_6S_{16}$	5806.74	1.33
${}_6S_{17}$	6020.71	1.13	${}_6S_{18}$	6238.10	1.38
${}_6S_{19}$	6446.15	1.76	${}_6S_{20}$	6653.89	1.31
${}_6S_{21}$	6855.20	1.80	${}_6S_{22}$	7050.31	1.64
${}_6S_{23}$	7234.75	1.48	${}_6S_{24}$	7412.49	2.08
${}_6S_{25}$	7588.13	2.01	${}_6S_{26}$	7756.13	2.10
${}_6S_{27}$	7921.94	1.63	${}_6S_{28}$	8088.18	2.04
${}_6S_{29}$	8255.78	2.03	${}_6S_{30}$	8417.21	2.07
${}_6S_{31}$	8588.30	2.65	${}_6S_{32}$	8759.31	3.13
${}_6S_{33}$	8926.92	2.62	${}_6S_{34}$	9092.08	2.92
${}_6S_{35}$	9257.99	3.61	${}_6S_{36}$	9423.84	3.10
${}_6S_{37}$	9599.31	2.31	${}_6S_{38}$	9760.55	2.99
${}_6S_{39}$	9928.85	2.27	${}_6S_{40}$	10 088.84	3.57
${}_7S_{12}$	5069.25	1.53	${}_7S_{17}$	6610.15	3.77
${}_7S_{19}$	6919.81	4.48	${}_7S_{20}$	7077.02	3.61
${}_7S_{21}$	7248.37	2.82	${}_7S_{22}$	7418.73	1.96
${}_7S_{23}$	7593.92	1.68	${}_7S_{24}$	7778.87	2.24
${}_7S_{25}$	7964.31	2.73	${}_7S_{26}$	8154.33	2.26
${}_7S_{27}$	8342.30	1.70	${}_7S_{28}$	8522.63	1.99
${}_7S_{29}$	8712.29	2.08	${}_7S_{30}$	8902.52	2.35
${}_7S_{31}$	9089.29	2.74	${}_7S_{32}$	9279.15	2.30
${}_7S_{33}$	9457.46	2.07	${}_7S_{34}$	9636.83	2.67
${}_7S_{35}$	9820.29	2.70	${}_7S_{36}$	9998.50	3.37
${}_7S_{37}$	10 174.04	3.68	${}_7S_{38}$	10 347.65	3.28
${}_7S_{39}$	10 528.43	4.93	${}_7S_{40}$	10 710.29	4.15
${}_8S_{10}$	5506.78	0.62	${}_8S_{11}$	5709.54	1.99
${}_8S_{21}$	7976.33	4.25	${}_8S_{22}$	8127.86	4.39
${}_9S_{10}$	5605.54	1.51	${}_9S_{11}$	5880.83	0.83
${}_9S_{12}$	6185.07	0.85	${}_9S_{13}$	6479.69	0.82
${}_9S_{14}$	6766.30	1.00	${}_9S_{15}$	7026.49	1.09
${}_9S_{16}$	7232.73	2.51	${}_9S_{18}$	7541.47	3.86

Table 2. (*Continued.*)

Mode	f	σ	Mode	f	σ
${}_{10}S_{10}$	6185.10	1.39	${}_{10}S_{11}$	6446.66	2.06
${}_{10}S_{12}$	6687.90	2.06	${}_{10}S_{13}$	6863.79	2.85
${}_{10}S_{15}$	7195.04	2.54	${}_{10}S_{16}$	7420.12	1.52
${}_{10}S_{17}$	7673.49	1.37	${}_{10}S_{18}$	7936.46	1.09
${}_{10}S_{19}$	8195.52	1.08	${}_{10}S_{20}$	8444.79	1.33
${}_{10}S_{21}$	8675.90	2.33	${}_{10}S_{22}$	8864.67	2.44
${}_{10}S_{26}$	10 036.77	2.13	${}_{10}S_{27}$	10 254.54	2.60
${}_{10}S_{28}$	10 459.85	3.05	${}_{10}S_{29}$	10 649.34	3.20
${}_{11}S_{10}$	6706.02	1.22	${}_{11}S_{20}$	8724.19	4.78
${}_{11}S_{21}$	8896.96	3.35	${}_{11}S_{22}$	9103.06	2.35
${}_{11}S_{23}$	9327.23	1.84	${}_{11}S_{24}$	9572.88	2.12
${}_{11}S_{28}$	10 795.57	4.36	${}_{11}S_{29}$	10 998.78	3.40
${}_{11}S_{30}$	11 220.57	2.26	${}_{11}S_{31}$	11 421.86	3.76
${}_{11}S_{32}$	11 643.02	3.02	${}_{11}S_{33}$	11 861.82	3.33
${}_{11}S_{34}$	12 052.86	3.18	${}_{12}S_{11}$	7135.66	0.89
${}_{12}S_{12}$	7449.36	0.79	${}_{12}S_{13}$	7767.92	0.64
${}_{12}S_{14}$	8088.30	0.83	${}_{12}S_{15}$	8402.99	0.97
${}_{12}S_{16}$	8689.38	1.77	${}_{13}S_{16}$	8741.38	1.53
${}_{13}S_{17}$	9053.82	1.56	${}_{13}S_{18}$	9365.05	1.40
${}_{13}S_{19}$	9663.55	1.06	${}_{13}S_{20}$	9953.63	1.40
${}_{13}S_{21}$	10 226.24	1.70	${}_{13}S_{22}$	10 476.61	2.03
${}_{15}S_{11}$	8122.42	1.09	${}_{15}S_{12}$	8426.74	1.30
${}_{15}S_{15}$	9595.53	1.31	${}_{15}S_{16}$	9921.25	1.82
${}_{16}S_{18}$	10 626.13	1.38	${}_{16}S_{19}$	10 958.29	1.68
${}_{16}S_{20}$	11 278.91	1.56	${}_{16}S_{21}$	11 578.49	3.01
${}_{17}S_{22}$	11 970.57	3.51	${}_{17}S_{23}$	12 257.32	1.72
${}_{17}S_{24}$	12 547.61	1.30	${}_{17}S_{25}$	12 833.44	2.05
${}_{19}S_{13}$	10 419.69	2.12	${}_{19}S_{14}$	10 710.43	2.06
${}_{19}S_{15}$	10 991.57	1.90	${}_{20}S_{19}$	12 323.64	1.89

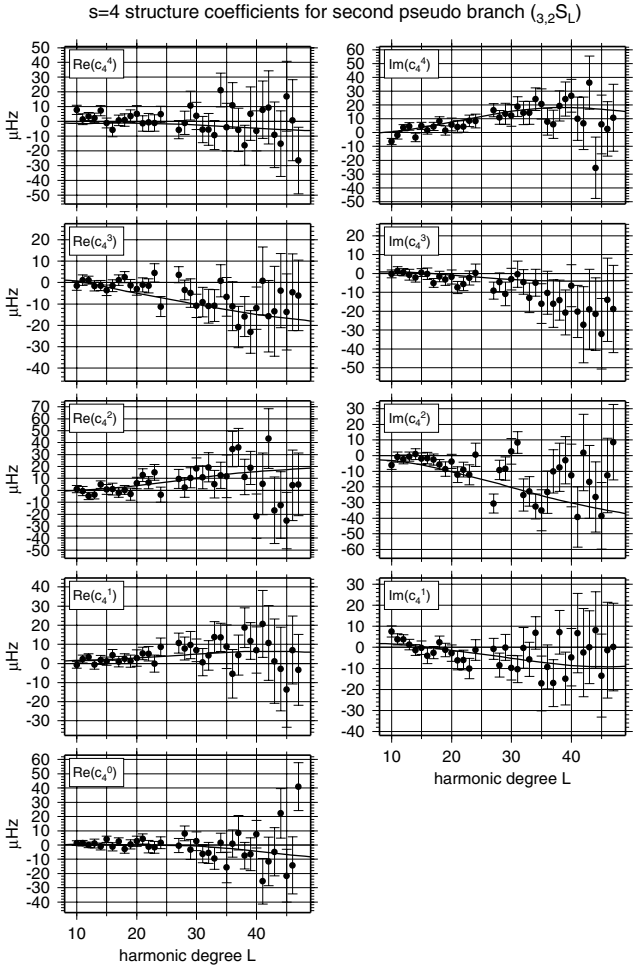

Figure 11. Same as in Fig. 9 but for structure of degree $s=4$ and for the second pseudo-branch: ${}_3S_\ell$ for $\ell<25$ and ${}_2S_\ell$ for $\ell>25$. Mode eigenfunctions along this pseudo-branch vary smoothly and hence we also expect the structure coefficients to exhibit smooth variations with ℓ. Model SCB10L18 seems to predict this branch very well.

modes (He & Tromp 1996; Resovsky & Ritzwoller 1998, and G. Masters, private communication 1998) we find 21 (27) sEd with a relative error of less than 1 per cent (10 per cent). When combined with the data set of this study we arrive at a new data set with 342 mantle-sensitive modes. For this data set we find 55 sEd with a precision better than 1 per cent. While these numbers are calculated for the structure coefficient $\mathrm{Im}(c_2^2)$, they remain essentially unchanged for other azimuthal orders t and harmonic degree $s=2$.

8 CONCLUSIONS

We have presented a new technique to retrieve both aspherical structure coefficients and multiplet degenerate frequencies from overtones with harmonic degree greater than 10. While degenerate frequency estimates for these modes have been obtained in previous studies using the regular multiplet stripping technique, such estimates were very probably biased due to uneven data coverage.

As far as the newly obtained structure coefficients are concerned we hope that other techniques can also be extended to high harmonic degree overtones. This would provide an independent check on our results.

While estimation of the longest-wavelength density structure independent of seismic P and S velocities has been attempted recently (Ishii & Tromp 1999, 2001), the ability of current structure coefficient data sets to resolve such density structure remains controversial (Masters *et al.* 2000). Considering that the new structure coefficients presented here all come from relatively high-frequency modes—the median degenerate frequency is 7.5 mHz—we expect that they only make a modest contribution to resolving mantle density structure.

However, the new observations should provide valuable additional constrains for both the construction of new spherically symmetric reference earth models and models of the longest-wavelength *P*- and *S*-velocity mantle structure.

A complete list of the estimated structure coefficients for degrees $s=2$, 4 is available both at http://www.geophys.uni-stuttgart.de/~widmer and the REM (Reference Earth Model) website http://mahi.ucsd.edu/Gabi/rem.html. The websites include also a machine-readable version of Table 2, branch plots similar to forallbranches Figs 8–11, for all branches and the peak shift patterns as in Figs 6 and 7 for all multiplets.

ACKNOWLEDGMENTS

The author wishes to acknowledge IRIS, GEOSCOPE, MEDNET and GEOFON for the high-quality data used in this study; Guy Masters for the SCB10L18 predictions and the spherical harmonic spline code; Gabi Laske for Crust5.1 structure coefficients; Freeman Gilbert for many stimulating

discussions; Pete Davis for encouraging me to work on this problem and both Barbara Romanowicz and Jeroen Tromp for constructive reviews. Financial support was provided by the National Science Foundation (NSF) undergrant EAR 94-18242. Additional funds were provided by the Cecil and Ida Green foundation for the Earth sciences and a grant from the NSF-CSEDI programme (EAR-09706).

REFERENCES

Backus, G., 1964. Geographical interpretation of measurements of average phase velocities of surface waves over great circular and great semicircular paths, *Bull. seism. Soc. Am.,* **54,** 571–610.

Cara, M., 1973. Filtering of dispersed wavetrains, *Geophys. J. R. astr. Soc.,* **33,** 65–80.

Cara, M., 1979. Lateral variations of S velocity in the upper mantle from higher Rayleigh modes, *Geophys. J. R. astr. Soc.,* **57,** 649–670.

Dahlen, F., 1982. The effect of data windows on the estimation of free oscillation parameters, *Geophys. J. R. astr. Soc.,* **69,** 537–549.

Dahlen, F. & Sailor, R., 1979. Rotational and elliptical splitting of the free oscillations of the earth, *Geophys. J. R. astr. Soc.,* **58,** 609–623.

Dahlen, F. & Tromp, J., 1998. *Theoretical Global Seismology,* Princeton University Press, Princeton, NJ.

Dziewonski, A. & Anderson, D., 1981. Preliminary reference Earth model, *Phys. Earth planet. Inter.,* **25,** 297–356.

Efron, B. & Tibshirani, R., 1986. Bootstrap methods for standard errors, confidence intervals, and other measures of statistical accuracy, *Statistical Sci.,* **1,** 54–77.

Ekström, G., Tromp, J. & Larson, E.W.F., 1997. Measurements and global models of surface wave propagation, *J. geophys. Res.,* **102,** 8137–8157.

Giardini, D., Li, X.-D. & Woodhouse, J., 1987. Three-dimensional structure of the earth from splitting in free oscillation spectra, *Nature,* **325,** 405–411.

Giardini, D., Li, X.-D. & Woodhouse, J., 1988. Splitting functions of long period normal modes of the earth, *J. geophys. Res.,* **93,** 13 716–13 742.

Gilbert, F., 1971. Ranking and winnowing gross earth data for inversion and resolution, *Geophys. J. R. astr. Soc.,* **23,** 125–128.

Gilbert, F. & Dziewonski, A., 1975. An application of normal-mode theory to the retrieval of structural parameters and source mechanisms from seismic spectra, *Phil. Trans. R. Soc. Lond.,* **A278,** 187–269.

Golub, G. & Reinsch, C., 1971. Singular value decompositions and least squares solutions, in *Linear Algebra,* pp. 134–151, eds. Wilkinson, J.H. & Reinsch, C., Springer Verlag, New York.

He, X. & Tromp, J., 1996. Normal mode constraints on the structure of the mantle and core, *J. geophys. Res.,* **101,** 20 053–20 082.

Ishii, M. & Tromp, J., 1999. Normal-mode and free air gravity constraints on lateral variations in velocity and density of the Earth's mantle, *Science,* **285,** 1231–1236.

Ishii, M. & Tromp, J., 2001. Even-degree lateral variations in the earth's mantle constrained by free oscillations and free-air gravity anomaly, *Geophys. J. Int.,* **145,** 77–96.

Jordan, T., 1978. A procedure for estimating lateral variations from low-frequency eigenspectra data, *Geophys. J. R. astr. Soc.,* **52,** 441–455.

Laske, G. & Masters, G., 1996. Constraints on global phase velocity maps from long-period polarization data, *J. geophys. Res.,* **101,** 16 059–16 075.

Masters, G. & Gilbert, F., 1983. Attenuation in the Earth at low frequencies, *Phil. Trans. R. Soc. Lond.,* **A308,** 479–522.

Masters, G., Jordan, T., Silver, P. & Gilbert, F., 1982. Aspherical earth structure from fundamental spheroidal-mode data, *Nature,* **298,** 609–613.

Masters, G., Laske, G. & Gilbert, F., 1999. Autoregressive estimation of the splitting matrix of free oscillation multiplets, *Geophys. J. Int.,* **141,** 25–42.

Masters, G., Laske, G. & Gilbert, F., 2000. Matrix autoregressive analysis of free-oscillation coupling and splitting, *Geophys. J. Int.,* **143,** 478–489.

Montagner, J.-P. & Tanimoto, T., 1990. Global anisotropy in the upper mantle inferred from the regionalization of phase velocities, *J. geophys. Res.,* **95,** 4797–4819.

Mooney, W., Laske, G. & Masters, G., 1998. Crust5.1: a global model at 5×5, *J. geophys. Res.,* **103,** 727–747.

Nolet, G., 1975. Higher Rayleigh modes in western Europe, *Geophys. Res. Lett.,* **2,** 60–62.

Parker, R., 1989. *Geophysical Inverse Theory,* Princeton University Press, Princeton, NJ.

Resovsky, J. & Ritzwoller, M., 1998. New and refinded constraints on the three-dimensional earth structure from normal modes below 3 mHz, *J. geophys. Res.,* **103,** 783–810.

Ritzwoller, M., Masters, G. & Gilbert, F., 1986. Observations of anomalous splitting and their interpretation in terms of aspherical structure, *J. geophys. Res.,* **91,** 10 203–10 228.

Ritzwoller, M., Masters, G. & Gilbert, F., 1988. Constraining aspherical structure with low frequency interaction coefficients: application to uncoupled multiplets, *J. geophys. Res.,* **93,** 6369–6396.

Romanowicz, B. & Roult, G., 1986. First-order asymptotics for the eigenfrequencies of the Earth and application to the retrieval of large-scale lateral variations of structures, *Geophys. J. R. astr. Soc.,* **87,** 209–239.

Roult, G., Montagner, J.P. & Romanowicz, B., 1990. 3-D upper mantle shear velocity and attenuation from fundamental mode free oscillation data, *Geophys. J. Int.,* **101,** 61–80.

Smith, M. & Masters, G., 1989. Aspherical structure constraints from free oscillation frequency and attenuation measurements, *J. geophys. Res.,* **94,** 1953–1976.

Stutzmann, E. & Montagner, J.P., 1993. An inverse technique for retrieving higher mode phase velocity and mantle structure, *Geophys. J. Int.,* **113,** 669–683.

Stutzmann, E. & Montagner, J.P., 1994. Tomography of the transition zone from the inversion of higher mode surface waves, *Phys. Earth planet. Inter.,* **86,** 99–115.

Trampert, J. & Woodhouse, J., 1995. Global phase velocity maps of Love and Rayleigh waves between 40 and 150 seconds, *Geophys. J. Int.,* **122,** 675.

van Heijst, H.J. & Woodhouse, J., 1997. Measuring surface-wave overtone phase velocities using a mode-branch stripping technique, *Geophys. J. Int.,* **131,** 209–230.

van Heijst, H.J. & Woodhouse, J., 1999. Global high-resolution phase velocity distributions of overtone and fundamental-mode surface waves determined by mode branch stripping, *Geophys. J. Int.,* **137,** 601–620.

Widmer, R., Masters, G. & Gilbert, F., 1992. Observably split multiplets—data analysis and interpretation in terms of large-scale aspherical structure, *Geophys. J. Int.,* **111,** 559–576.

Wong, Y., 1989. Upper mantle heterogeneity from phase and amplitude data of mantle waves, *PhD thesis,* Harvard University, Cambridge, MA.

Woodhouse, J. & Dahlen, F., 1978. The effect of a general aspherical perturbation on the free oscillations of the earth, *Geophys. J. R. astr. Soc.,* **53,** 335–354.

Woodhouse, J. & Dziewonski, A., 1984. Mapping of the upper mantle: three-dimensional modeling of earth structure by inversion of seismic waveforms, *J. geophys. Res.,* **89,** 5953–5986.

Woodhouse, J. & Dziewonski, A., 1986. Three dimensional mantle models based on mantle wave and long period body wave data, *EOS Trans. AGU,* **67,** 307.